Sensorless Indirect-Rotor-Field-Orientation Speed Control of a Permanent-Magnet Synchronous Motor With Stator-Resistance Estimation

Mohamed Rashed, Peter F. A. MacConnell, A. Fraser Stronach, and Paul Acarnley

***Abstract*—Efficient and precise sensorless speed control of a permanent-magnet synchronous motor (PMSM) requires accurate knowledge of rotor flux, position, and speed. In the literature, many sensorless schemes have been presented, in which the accurate estimation of rotor flux magnitude, position, and speed is guaranteed by detecting the back electromotive force (EMF). However, these schemes show great sensitivity to stator resistance mismatch and system noise, particularly, during low-speed operation. In this paper, an indirect-rotor-field-oriented-control scheme for sensorless speed control of a PMSM is proposed. The rotor-flux position is estimated by direct integration of the estimated rotor speed to reduce the effect of the system noise. The stator resistance and the rotor-flux speed and magnitude are estimated adaptively using stable model reference adaptive system estimators. Simple stability analysis and design of the estimators are performed using linear-control theory applied to an error model of the PMSM in a synchronous rotating reference frame. The convergence of rotor position- and speed-estimation errors to zero is guaranteed. Experimental results show excellent performance.**

***Index Terms*—Parameters identification, permanent-magnet synchronous motor (PMSM), sensorless control, speed control.**

NOMENCLATURE

$\overline{\psi}_r$	Rotor-flux space vector.
$\overline{\boldsymbol{i}}_s$	Stator-current space vector.
$\overline{\boldsymbol{u}}_s$	Stator-voltage space vector.
ω_r	Rotor angular speed in electrical radians per second.
ρ_r	Rotor position.
ω_e	Synchronous rotating-reference-frame speed in electrical radians per second.
ρ_e	Position of synchronous rotating reference frame in electrical radians.
ψ_r	Actual rotor (magnet)-flux magnitude.
R_s	Stator-winding resistance.
L_s	Stator-winding inductance.
x, s	Subscripts, real, and imaginary components in synchronous rotating reference frame.
α, β	Subscripts, real, and imaginary components in stator reference frame.

Manuscript received April 6, 2005; revised January 3, 2006.

M. Rashed is with the Electrical Engineering Department, Mansoura University, Mansoura 35516, Egypt (email: m.rashed@eng.abdn.ac.uk).

P. F. A. MacConnell is with the School of Engineering and Physical Sciences, University of Aberdeen, Aberdeen, AB24 3UE, U.K.

A. F. Stronach was with the School of Engineering and Physical Sciences, University of Aberdeen, Aberdeen, AB24 3UE, U.K. He is now with Genbase Information Systems, Aberdeen, AB24 3UE, U.K.

P. Acarnley is with the School of Engineering, Robert Gordon University, Aberdeen, AB10 1FR, U.K., and also with the University of Aberdeen, Aberdeen, AB24 3UE, U.K.

Digital Object Identifier 10.1109/TIE.2007.895136

I. INTRODUCTION

PERMANENT-MAGNET synchronous motors (PMSMs) are known to provide higher torque per unit volume and better efficiency than induction motors, while improvements in the properties of permanent-magnet materials have increased their viability. Recently, sensorless PMSM drives have received increasing interest for industrial applications where there are limitations on the use of a position sensor. The elimination of the position sensor reduces the cost of the drive and increases the overall system ruggedness and reliability. High-performance operation of sensorless PMSM drives mainly relies on accurate knowledge of the rotor-magnet flux magnitude, position, and speed. The sensorless rotor-position estimation techniques can be classified into two major groups: the motor-model-based and the rotor-saliency-based techniques. The latter are suitable only for the interior PMSM (IPMSM). Most of the motor-model-based techniques detect the back-EMF vector, which holds information about the rotor position and speed, using either open-loop estimators [1]–[3] or closed-loop estimators/observers [4]–[9]. In other motor-model-based techniques, the rotor-flux vector is directly estimated [10], [11]. Moreover, adaptive observers have been used to estimate the stator current, the rotor speed, and the rotor position [12]–[15]. Extended Kalman filters (EKF) have also been proposed for rotor speed and position estimation [16], [17]. Although the EKF algorithm is stable and well known, the EKF is computationally intensive and requires proper initialization. Furthermore, model reference adaptive system (MRAS) has been used extensively for combined rotor flux and speed estimation in induction motors [18].

In [1], open-loop back-EMF-based position and speed estimators have been considered. The scheme is sensitive to the system noise and to the stator resistance mismatch. In [4], the rotor-flux vector is estimated by direct integration of the calculated back EMF. The estimated rotor-flux vector is corrected adaptively by utilizing the error between measured and estimated stator currents to reduce the effect of integration drift. However, the scheme is not suitable for low-speed operation. On the other hand, in [12], an identity observer has been proposed to estimate the rotor speed by utilizing the

stator-current estimation error, provided that the rotor-flux magnitude is known. The rotor position is estimated by integrating the estimated rotor speed to reduce the effect of the system measurement noise. A similar nonlinear full-order observer is employed for speed estimation in the study in [15], where the pole-placement technique is used to locate the observer's eigenvalues. Although, the convergence of the estimated rotor position to its true value is guaranteed, the scheme is sensitive to stator-resistance and rotor-flux magnitude mismatch.

In [14], a sensorless adaptive full-state observer incorporating a motor mechanical model has been developed. The stator current, the rotor speed, and the rotor position are estimated. Moreover, the parameters of the mechanical model are adaptively estimated and used for online pole placement of the motor controller. A series of papers has been published by Solsona [5], [6], [13], in which the rotor position and speed are estimated using the mechanical and electrical models of the PMSM. In [5], a reduced order observer has been presented, in which the back-EMF vector in the stator reference frame is observed. The rotor position and speed are, then, algebraically calculated using the two back-EMF-vector components. This method of calculation introduces measurement noise directly to the estimated position and speed signals. In [13], an extended observer has been proposed to estimate the stator current, the rotor position, the rotor speed, and the load torque. The observer shows sensitivity to electrical parameter variations that may lead to unstable operation.

Some authors have used a two-time-scale approach, where the drive's mechanical model variables are assumed to be slowly varying as compared to the electrical variables, i.e., ω_r is assumed constant. Therefore, only the electrical model of the PMSM is used to estimate the rotor position and speed [7]–[11]. A disturbance observer has been proposed to estimate the back EMF, from which the rotor position is directly estimated [7]. An independent adaptive rotor-speed estimator is also used. It has been shown that the observer suffers from steady-state position-estimation error [6]. In [10], a sliding-mode observer has been developed to estimate the rotor-flux vector instead of the back EMF. In addition, in [11], a flux-state observer has been developed to estimate the rotor flux; however, the observer is sensitive to stator resistance mismatch. In [8] and [9], a disturbance observer has been applied to the IPMSM to estimate the back EMF. The motor speed is adaptively and independently estimated. It has been shown that these observers are sensitive to mismatch between the actual value of stator resistance and the value of resistance assumed in the electrical model. This mismatch has greatest effect at low speeds and high loads, where the voltage drop across the stator resistance is large in comparison to the back EMF.

It is now clear that sensorless rotor-flux estimation using the machine model is still problematic at low speeds. The main limitations arise from the observability problem when operating at zero speed and the sensitivity to stator resistance mismatch at low speed. Moreover, direct estimation of the rotor position from the estimated back-EMF vector introduces measurement noise directly into the position estimate. During operation, the stator resistance increases while the rotor magnet flux decreases due to the motor-temperature rise. However, the rate of change of the stator resistance per degree Celsius is much greater than the rate of change of the rotor magnet flux. The stator resistance may increase by a value up to 50% of its nominal value during operation. This large percentage of resistance mismatch severely affects the accuracy of the estimated rotor-flux vector and may lead to unstable operation at speeds close to zero [15]. Thus, for low-speed operation, it is much more important to update online the stator resistance than the rotor flux.

In this paper, an indirect-rotor-field-oriented control (IRFOC) scheme for a PMSM is proposed. The new scheme is insensitive to the stator resistance mismatch. The rotor-flux vector is estimated in its polar form, where the rotor-flux vector is completely defined by its magnitude and position. The electrical model of the motor is used to estimate the rotor-flux vector, assuming ω_r, and the rotor-flux magnitude are slowly varying parameters. Three MRAS estimators are designed to estimate the rotor speed, the rotor-flux magnitude, and the stator resistance. The rotor-flux position is estimated by direct integration of the estimated speed to reduce the effect of measurement noise. It is demonstrated that the simultaneous estimation of the stator resistance and the rotor-flux magnitude is not possible, so two separate estimation schemes are proposed. In Scheme 1, MRAS stator-resistance and rotor-speed estimators are used, while the rotor-flux magnitude is set to its nominal value. In Scheme 2, the rotor-flux magnitude and the rotor speed are estimated adaptively using MRAS estimators, while the stator resistance is set to its nominal value. Scheme 1 is shown to provide stable and robust operation at low speeds. The MRAS estimators are designed to provide stable operation when used independently and simultaneously. Stability analysis and design of the MRAS estimators have been performed for a PMSM error model in a synchronous rotating reference frame fixed to the estimated rotor-flux vector. The convergence of the estimated rotor position and speed to their true values is also guaranteed.

The model of the PMSM in stationary and synchronous rotating reference frames is discussed in Section II. In Section III, sensorless adaptive rotor-flux-vector estimation Schemes 1 and 2 are designed and discussed. Experimental results for both schemes are presented in Section IV.

II. PMSM Model

The linear state-space model of a surface-mounted PMSM in a stationary reference frame $(\mathrm{s}\alpha, \mathrm{s}\beta)$, which is fixed to the stator windings, is given as [10]

$$\dot{\overline{\boldsymbol{\psi}}}_r = \boldsymbol{J}\omega_r\overline{\boldsymbol{\psi}}_r \tag{1a}$$

$$\dot{\bar{i}}_s = -a_1\boldsymbol{I}\bar{\boldsymbol{i}}_s - \boldsymbol{J}a_2\omega_r\overline{\boldsymbol{\psi}}_r + a_2\bar{\boldsymbol{u}}_s \tag{1b}$$

where

$$\overline{\boldsymbol{u}}_s = [u_{s\alpha} \quad u_{s\beta}]^{\mathrm{T}}, \quad \bar{\boldsymbol{i}}_s = [i_{s\alpha} \quad i_{s\beta}]^{\mathrm{T}},$$

$$\overline{\boldsymbol{\psi}}_r = [\psi_{r\alpha} \quad \psi_{r\beta}]^{\mathrm{T}}, \quad \psi_r = \sqrt{\psi_{r\alpha}^2 + \psi_{r\beta}^2}$$

$$\psi_{r\alpha} = \psi_r \cos\rho_r, \quad \psi_{r\beta} = \psi_r \sin\rho_r,$$

$$\rho_r = \int \omega_r dt, \quad a_1 = \frac{R_s}{L_s}, \quad a_2 = \frac{1}{L_s},$$

$$\boldsymbol{J} = \begin{bmatrix} 0 & -1 \\ 1 & 0 \end{bmatrix}, \quad \text{and} \quad \boldsymbol{I} = \begin{bmatrix} 1 & 0 \\ 0 & 1 \end{bmatrix}.$$

The motor-state variables are the two stator currents $i_{s\alpha}$ and $i_{s\beta}$ and two rotor fluxes $\psi_{r\alpha}$ and $\psi_{r\beta}$. The system inputs are the stator voltages $u_{s\alpha}$ and $u_{s\beta}$. The system outputs are $i_{s\alpha}$ and $i_{s\beta}$. Equation (1b) represents the motor-stator-circuit model. Equation (1a) represents the rotor model, which is completely decoupled from (1b), since the rotor flux is provided by a permanent magnet. Practically, because of drift and initialization difficulties, the rotor-flux vector cannot be estimated by using the rotor model (1a). Therefore, the rotor-flux vector is estimated/observed by utilizing the error between the measured and estimated stator currents using (1b). It is well known that the design and analysis of estimators/observers in the synchronous rotating reference frames is much simpler than in the stator reference frame, since in the synchronous reference frame, the sinusoidal time varying variables of the PMSM are transformed to dc variables. In a synchronous rotating reference frame (x, y) that rotates at speed ω_e, the motor model in (1) is written as

$$\dot{\overline{\boldsymbol{\psi}}}_r = -\boldsymbol{J}(\omega_{sl})\overline{\boldsymbol{\psi}}_r \tag{2a}$$

$$\dot{\bar{\boldsymbol{i}}}_s = -(a_1\boldsymbol{I} + \omega_e\boldsymbol{J})\bar{\boldsymbol{i}}_s - \boldsymbol{J}a_2\omega_r\overline{\boldsymbol{\psi}}_r + a_2\overline{\boldsymbol{u}}_s \tag{2b}$$

where

$$\overline{\boldsymbol{u}}_s = [u_{sx} \quad u_{sy}]^{\mathrm{T}}, \quad \bar{\boldsymbol{i}}_s = [i_{sx} \quad i_{sy}]^{\mathrm{T}},$$

$$\overline{\boldsymbol{\psi}}_r = [\psi_{sx} \quad \psi_{sy}]^{\mathrm{T}}, \quad \psi_r = \sqrt{\psi_{rx}^2 + \psi_{ry}^2},$$

$$\omega_e = \frac{d}{dt}\rho_e, \quad \text{and} \quad \omega_{sl} = (\omega_e - \omega_r).$$

III. Adaptive Rotor-Flux-Vector Estimator

In the synchronous rotating reference frame, the estimated version of the PMSM model in (2) may be expressed as follows:

$$\dot{\hat{\overline{\boldsymbol{\psi}}}}_r = -\boldsymbol{J}(\hat{\omega}_{sl})\hat{\overline{\boldsymbol{\psi}}}_r \tag{3a}$$

$$\dot{\hat{\bar{\boldsymbol{i}}}}_s = -(\hat{a}_1\boldsymbol{I} + \omega_e\boldsymbol{J})\hat{\bar{\boldsymbol{i}}}_s - \boldsymbol{J}a_2\hat{\omega}_r\hat{\overline{\boldsymbol{\psi}}}_r + a_2\overline{\boldsymbol{u}}_s \tag{3b}$$

where $\hat{\omega}_{sl} = (\omega_e - \hat{\omega}_r)$, and "$\wedge$" denotes an estimated quantity.

By subtracting (3a) and (3b) from (2a) and (2b), respectively, and by applying the Laplace transformation, an estimation-error model of the PMSM in the synchronous rotating reference frame and in matrix form is given as

$$\begin{bmatrix}\Delta\psi_{rx}\\ \Delta\psi_{ry}\end{bmatrix} = \frac{1}{s^2+\omega_{sl}^2}\begin{bmatrix}(-\hat{\psi}_{ry}s + \omega_{sl}\hat{\psi}_{rx})\\ (\hat{\psi}_{rx}s + \omega_{sl}\hat{\psi}_{ry})\end{bmatrix}\Delta\omega_r \tag{4a}$$

$$\begin{bmatrix}\Delta i_{sx}\\ \Delta i_{sy}\end{bmatrix} = \frac{-1}{D}\left\{\begin{bmatrix}\hat{i}_{sx}F + \hat{i}_{sy}\omega_e\\ \hat{i}_{sy}F - \hat{i}_{sx}\omega_e\end{bmatrix}\Delta a_1 + a_2\begin{bmatrix}\hat{\psi}_{rx}\omega_e - \hat{\psi}_{ry}F\\ \hat{\psi}_{rx}F + \hat{\psi}_{ry}\omega_e\end{bmatrix}\Delta\omega_r + a_2\begin{bmatrix}\omega_r\omega_e & -\omega_rF\\ \omega_rF & \omega_r\omega_e\end{bmatrix}\begin{bmatrix}\Delta\psi_{rx}\\ \Delta\psi_{ry}\end{bmatrix}\right\} \tag{4b}$$

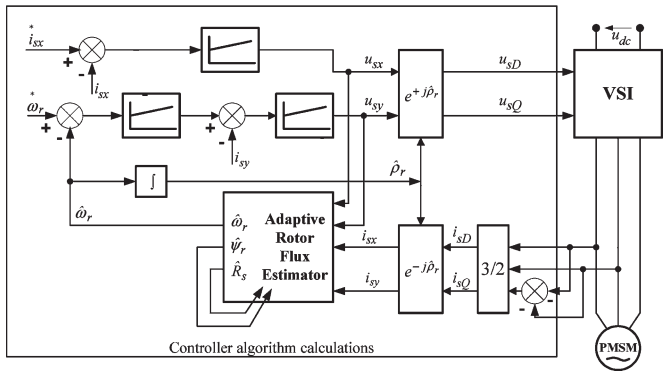

Fig. 1. Sensorless IRFOC PMSM drive.

where

$$\Delta\overline{\boldsymbol{\psi}}_r = \overline{\boldsymbol{\psi}}_r - \hat{\overline{\boldsymbol{\psi}}}_r = [\Delta\psi_{rx} \quad \Delta\psi_{ry}]^{\mathrm{T}},$$

$$\Delta\omega_r = (\omega_r - \hat{\omega}_r), \quad \Delta\bar{\boldsymbol{i}}_s = \bar{\boldsymbol{i}}_s - \hat{\bar{\boldsymbol{i}}}_s = [\Delta i_{sx} \quad \Delta i_{sy}]^{\mathrm{T}},$$

$$\Delta a_1 = (a_1 - \hat{a}_1) \quad \Delta i_{sx} = (i_{sx} - \hat{i}_{sx}),$$

$$\Delta i_{sy} = (i_{sy} - \hat{i}_{sy}), \quad \Delta\psi_{rx} = (\psi_{rx} - \hat{\psi}_{rx}),$$

$$\Delta\psi_{ry} = (\psi_{ry} - \hat{\psi}_{ry}), \quad \omega_r\overline{\boldsymbol{\psi}}_r - \hat{\omega}_r\hat{\overline{\boldsymbol{\psi}}}_r = \omega_r\Delta\overline{\boldsymbol{\psi}}_r + \Delta\omega_r\hat{\overline{\boldsymbol{\psi}}}_r,$$

$$D = F^2 + \omega_r^2, \quad \text{and} \quad F = (s + a_1).$$

The stator-current errors Δi_{sx} and Δi_{sy} are utilized to estimate the rotor speed (ω_r), the stator-resistance parameter (a_1), and the rotor-flux magnitude (ψ_r), using MRAS estimators. The actual PMSM drive (as a reference model) and its implemented model inside the drive controller (as an adjustable model) are operated in parallel. Inside the controller of the IRFOC PMSM drive, the synchronous rotating reference frame is assumed fixed to the estimated rotor-flux vector, and thus, the estimated rotor-flux-vector components are the following: $\hat{\psi}_{rx} = \hat{\psi}_r$ and $\hat{\psi}_{ry} = 0$. Therefore, from (3b), the estimates of the stator currents and the rotor position are implemented as follows:

$$\dot{\hat{i}}_{sx} = -\hat{a}_1\hat{i}_{sx} + \omega_e\hat{i}_{sy} + a_2u_{sx} \tag{5a}$$

$$\dot{\hat{i}}_{sy} = -\hat{a}_1\hat{i}_{sy} - \omega_e\hat{i}_{sx} - a_2\hat{\omega}_r\hat{\psi}_r + a_2u_{sy} \tag{5b}$$

$$\hat{\omega}_{sl} = 0 \quad \omega_e = \hat{\omega}_r \quad \hat{\rho}_r = \int\hat{\omega}_r dt. \tag{5c}$$

Fig. 1 shows the block diagram of the proposed sensorless IRFOC PMSM drive.

It should be noted that the estimated flux component $\hat{\psi}_{ry}$ is assumed known and equal to zero, while the estimated flux component $\hat{\psi}_{rx}$ is assumed equal to the magnitude of the estimated rotor-flux vector $\hat{\psi}_r$ and is unknown. In addition, $\omega_{sl} = -\Delta\omega_r$, since $\hat{\omega}_{sl}$ is equal to zero (5c). Furthermore, for small perturbations around the equilibrium point, $\Delta\omega_r$ is small, and thus, $\Delta\omega_r^2$ is negligible. Therefore, substituting $\omega_{sl}^2 = 0$ and $\hat{\psi}_{ry} = 0$ into (4) and eliminating $\Delta\psi_{ry}$ from (4b), yields

$$\begin{bmatrix}\Delta i_{sx}\\ \Delta i_{sy}\end{bmatrix} = \frac{1}{D}\left\{\begin{bmatrix}-\hat{i}_{sx}F - \hat{i}_{sy}\omega_r\\ -\hat{i}_{sy}F + \hat{i}_{sx}\omega_r\end{bmatrix}\Delta a_1 - a_2\begin{bmatrix}\omega_r^2\\ \omega_rF\end{bmatrix}\Delta\psi_{rx} + \frac{a_2}{s}\begin{bmatrix}a_1\omega_r\hat{\psi}_r\\ -\hat{\psi}_r\left(s^2 + a_1s + \omega_r^2\right)\end{bmatrix}\Delta\omega_r\right\}. \tag{6}$$

The stator-current-error components Δi_{sx} and $\Delta i_{s\psi}$ are functions only of the errors of the unknown parameters, which are $\Delta\omega_r$, Δa_1, and $\Delta\psi_{rx}$, and are utilized to derive the adaptive error signals ε_ω, ε_ψ, and ε_{a1}. The intention is to feed these error signals to polarization-index (PI)-type controllers to estimate adaptively the unknown parameters ω_r, ψ_r, and a_1. However, it is at this stage that a fundamental difficulty arises: it is not possible to derive values of the three independent variables $\Delta\psi_{rx}$, Δa_1, and $\Delta\omega_r$ in (6) in terms of the two variables, Δi_{sx} and Δi_{sy}. The remainder of this paper describes the techniques used to overcome this difficulty. The basic strategy is to use two separate schemes, each of which calculate just two of the three error signals (with the third signal assumed to be zero), with the choice of scheme depending on the instantaneous operating condition of the PMSM. Thus, in Scheme 1, $\hat{\psi}_r$ is set equal to its nominal value ψ_{r-n}, and the estimator adapts the rotor speed ω_r, and stator-resistance parameter a_1. As discussed in the Introduction, variation of the stator resistance is much more significant than variation of rotor flux at low speed, so Scheme 1 is most suitable for low-speed operation of the PMSM. Conversely, in Scheme 2, the stator-resistance parameter $\hat{a}_1$ is set equal to its nominal value a_{1-n}. Therefore, the Scheme-2 estimator adapts the rotor speed ω_r and rotor flux ψ_r, which is most appropriate for high-speed operation, where the stator-resistive voltage drop is small in comparison to the back EMF.

A. Simultaneous Estimation of Motor Speed and Stator Resistance: Scheme 1

From (6), the adaptive-error-signal equations of the rotor speed and the stator resistance are chosen as follows:

$$\varepsilon_\omega = -\frac{1}{a_2\hat{\psi}_r}\Delta i_{sy} \quad \varepsilon_{a1} = \frac{1}{\hat{i}_s^2\omega_r}(-\hat{i}_{sy}\Delta i_{sx} + \hat{i}_{sx}\Delta i_{sy}). \tag{7}$$

The adaptive-error-signal equations in (7) are chosen according to the following rules.

1) They should be a set of linearly independent equations in Δi_{sx} and Δi_{sy}.
2) The poles and the zeros of the transfer functions $(\varepsilon_\omega/\Delta\omega_r)$ and $(\varepsilon_{a1}/\Delta a_1)$ should be located in the left-hand side of the s-plane at any operating point.
3) The gains of these transfer functions should be unity.

The adaptive error signals are fed to PI-type controllers to estimate ω_r, a_1, while the estimated rotor-flux magnitude is set equal to the nominal value of the magnet flux ψ_{r-n}. Thus,

$$\hat{\omega}_r = G_{c\omega}\varepsilon_\omega \quad \hat{a}_1 = G_{ca1}\varepsilon_{a1} \quad \hat{\psi}_r = \psi_{r-n} \tag{8}$$

where $G_{c\omega} = k_{p\omega} + k_{i\omega}/s$, $G_{ca1} = k_{pa1} + k_{ia1}/s$. $k_{p\omega}$, $k_{i\omega}$, k_{pa1}, and k_{ia1} are the PI controllers gains.

1) Stability Analysis and Controller Design: By substituting from (6) about Δi_{sx} and Δi_{sy} into (7), ε_ω and ε_{a1} may be expressed as function of $\Delta\psi_{rx}$, Δa_1, and $\Delta\omega_r$ as follows:

$$\begin{bmatrix}\varepsilon_\omega\\ \varepsilon_{a1}\end{bmatrix} = \begin{bmatrix}G_{\omega\omega} & G_{\omega a1}\\ G_{a1\omega} & G_{a1a1}\end{bmatrix}\begin{bmatrix}\Delta\omega_r\\ \Delta a_1\end{bmatrix} + \begin{bmatrix}G_{\omega\psi}\\ G_{a1\psi}\end{bmatrix}\Delta\psi_{rx} \tag{9}$$

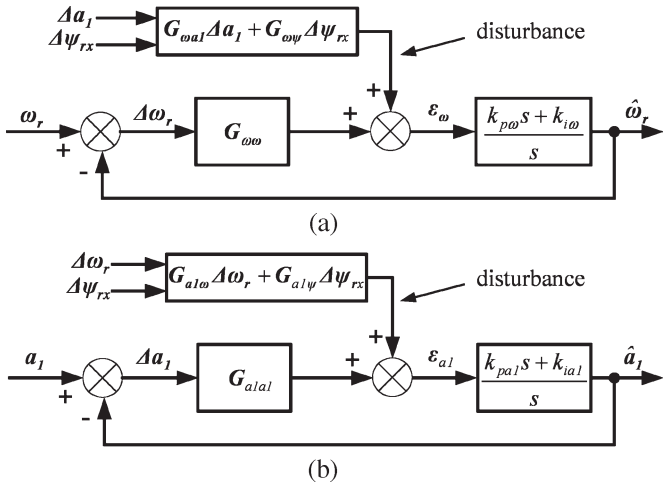

Fig. 2. Scheme-1 estimator block diagrams. (a) Rotor-speed estimator. (b) Stator-resistance estimator.

where

$$G_{\omega\omega} = \frac{\left(s^2 + a_1 s + \omega_r^2\right)}{sD},$$

$$G_{\omega\psi} = \frac{\omega_r F}{\hat{\psi}_r D}, \quad G_{\omega a1} = \frac{\hat{i}_{sy}F - \hat{i}_{sx}\omega_r}{a_2\hat{\psi}_r D},$$

$$G_{a1\omega} = -a_2\hat{\psi}_r\frac{\hat{i}_{sy}a_1\omega_r + \hat{i}_{sx}\left(s^2 + a_1 s + \omega_r^2\right)}{\hat{i}_s^2\omega_r sD},$$

$$G_{a1\psi} = a_2\frac{\hat{i}_{sy}\omega_r - \hat{i}_{sx}F}{\hat{i}_s^2 D}, \quad \text{and} \quad G_{a1a1} = \frac{1}{D}.$$

The rotor-speed and the stator-resistance estimators, which are given by (7)–(9), are represented by the 2×2 multiple-input–multiple-output (MIMO) closed-loop control system shown in Fig. 2. The design of the PI controller for each estimator is performed independently, with each estimator being treated as a single-input–single-output (SISO) closed-loop control system. As an example, the rotor-speed estimator is designed by assuming the effect of $\Delta\psi_{rx}$, and Δa_1 is a bounded external disturbance. From (9) and Fig. 2, since the poles and the zeros of transfer functions $G_{\omega\omega}$ and G_{a1a1} of the rotor speed and the stator resistance estimators, respectively, are located in the left-hand side of the s-plane, the estimator's PI controller gains can be selected as high as possible to provide quick tracking of the estimated variables. However, stability will not be guaranteed for simultaneous use of the estimators and needs to be investigated.

In the next sections, the speed and the stator-resistance estimators are designed independently. Afterwards, stability for simultaneous use will be investigated.

2) Speed-Estimator Design: The block diagram in Fig. 2(a) shows the closed-loop rotor-speed estimator. Before proceeding to determine the speed estimator's PI controller gains, it should be noted that the existence of a $G_{\omega\omega}$ pole at the origin of the s-plane ensures the convergence of $\Delta\omega_r$ to zero, whatever the value of the disturbance signal. This agrees with the physical interpretation that, at steady state, the rotor speed is

exactly equal to the estimated value, since ω_e is set equal to the estimated speed in the proposed IRFOC PMSM drive (5c). Thus, a simple proportional controller would be sufficient to ensure the convergence of $\Delta\omega_r$ to zero; although, ε_ω would not converge to zero. For this reason, a PI controller (with transfer function $G_{c\omega}$ and controller gains $k_{i\omega}$, $k_{p\omega}$) is used. The forward transfer function of the speed estimator [Fig. 2(a)] is

$$\hat{\omega}_r/\Delta\omega_r = G_{c\omega}G_{\omega\omega}. \tag{10}$$

It has four poles and three zeros. All are located in the left-hand side of the s-plane. Two of these poles, FFP1 and FFP2, are located at the origin, and the other two are conjugate poles, FFP3 and FFP4, with negative real part of $-a_1$ and imaginary part of ω_e. One of the three zeros is the PI controller zero FFZ1 and the other two are the zeros FFZ2 and FFZ3 of the transfer function $G_{\omega\omega}$. The feedforward gain is $k_{p\omega}$. The feedforward poles and zeros are the following: FFP1, $2 = 0$; FFP3, $4 = -a_1 \pm j\omega_e$; FFZ1 $= -k_{i\omega}/k_{p\omega}$; and FFZ2, $3 = -0.5a_1 \pm 0.5sqrt(a_1^2 - 4\omega_e^2)$.

The locations of the closed-loop transfer function poles characterize the control-system dynamics. The closed-loop speed estimator, which is shown in Fig. 2(a), has four poles. It was decided that the location of the PI controller zero FFZ1 should be on the real axis at $-a_1$ to make sure that the fast dynamic closed-loop poles are always located to the left of the conjugate poles FFP3-4, providing a quick transient response. The value of the proportional gain $k_{p\omega}$ can be selected to be as large as possible to give close tracking of the actual motor speed. The PI controller gains are chosen as follows: $k_{i\omega}/k_{p\omega} = a_1$ and $k_{p\omega} = 300$.

3) Stator-Resistance Estimator: The block diagram in Fig. 2(b) shows the closed-loop control system of the stator-resistance estimator. Similar to the speed estimator, the forward transfer function of the stator-resistance estimator is

$$\hat{a}_1/\Delta a_1 = G_{ca1}G_{a1a1}. \tag{11}$$

It has three poles FFP1-3 and one zero FFZ1. All are located in the left-hand side of the s-plane. The first pole FFP1 is at the origin. The other two poles are as follows: FFP2, $3 = -a_1 \pm j\omega_e$. The zero FFZ1 is the PI controller zero and is as follows: FFZ1 $= -k_{ia1}/k_{pa1}$. The FFZ1 is positioned close to the origin to reduce the dominance of the first closed-loop pole CLP1. k_{ia1}/k_{pa1} is selected equal to 20, and $k_{pa1} = 5000$.

4) MIMO Stability Investigation: The two estimators, which are shown in Fig. 2, have been designed independently by considering their separate open-loop transfer functions and selecting appropriate values of PI controller gains. However, changes in estimated outputs from either controller appear as disturbances in the other controller, so, therefore, the stability of the complete 2×2 MIMO system must be investigated. The stability analysis is performed by finding the locations of the closed-loop poles of the MIMO system. From Fig. 2, the relationship between the system outputs $\hat{\omega}_r$ and $\hat{a}_1$ and the errors $\Delta\omega_r$ and Δa_1, which represents the forward transfer function of the 2×2 MIMO system, is given as follows:

$$\begin{bmatrix} \hat{\omega}_r \\ \hat{a}_1 \end{bmatrix} = \begin{bmatrix} G_{c\omega} & 0 \\ 0 & G_{ca1} \end{bmatrix} \left\{ \begin{bmatrix} G_{\omega\omega} & G_{\omega a1} \\ G_{a1\omega} & G_{a1a1} \end{bmatrix} \times \begin{bmatrix} \Delta\omega_r \\ \Delta a_1 \end{bmatrix} + \begin{bmatrix} G_{\omega\psi} \\ G_{a1\psi} \end{bmatrix} \Delta\psi_{rx} \right\}. \tag{12}$$

The error $\Delta\psi_{rx}$ in (12) is assumed to be a bounded external disturbance, which is ignored for the purposes of the stability study. The closed-loop poles are obtained by solving the characteristic equation

$$\left| \boldsymbol{I} + \begin{bmatrix} G_{c\omega} & 0 \\ 0 & G_{ca1} \end{bmatrix} \begin{bmatrix} G_{\omega\omega} & G_{\omega a1} \\ G_{a1\omega} & G_{a1a1} \end{bmatrix} \right| = 0 \tag{13}$$

which reduces to

$$1 + G_{c\omega}G_{\omega\omega} + G_{ca1}G_{a1a1} + G_{c\omega}G_{ca1} \times [G_{\omega\omega}G_{a1a1} - G_{\omega a1}G_{a1\omega}] = 0. \tag{14}$$

The characteristic (14) is on the seventh order, and thus, it is difficult to determine analytically the stability conditions. However, one of the conditions of the Routh stability criteria is that the coefficients of the characteristic equation polynomial should be positive. Since, by inspection, the coefficients of the terms $G_{c\omega}G_{\omega\omega}$, $G_{ca1}G_{a1a1}$, and $G_{c\omega}G_{ca1}$ in (14) are positive, the Routh stability condition exists if the coefficients of the fourth term $[G_{\omega\omega}G_{a1a1} - G_{\omega a1}G_{a1\omega}]$ are also positive. It can be shown that this condition is met if

$$\hat{i}_{sx} = 0 \quad \text{or} \quad \text{sgn}(\hat{i}_{sx}) = \text{sgn}(\hat{i}_{sy}\omega_r). \tag{15}$$

In fact, i_{sx} is usually set equal to zero for operation at speeds below the base value, and this condition is imposed for all of the results in this paper. The conditions in (15) are validated by investigating numerically the locations of the closed-loop poles for the various operating modes of the drive. For example, Fig. 3 shows the loci of the closed-loop poles when $i_{sx} = 0$ A and $i_{sy} = 2$ A for a range of speed starting at ± 0.1 up to ± 314 elect. rad/s for the motor parameters given in Appendix A. The points indicated by crosses in Fig. 3 are the locations of the seven poles of the characteristic equation at $\omega_r = \pm 0.1$ elect. rad/s. As the speed increases, the poles' locations move in the directions indicated by the arrows. The loci obtained shows stable operation for the whole speed range in motoring and generating modes of operation. In conclusion, although the two estimators proposed are stable when used independently, interaction between the two estimators result in the overall scheme having the possibility of instability at low speeds. Specifically, the conditions in (15) should be considered to obtain stable operation at low speeds, but for high speeds, i_{sx} can be set to any value. The convergence of the Scheme-1 estimators is investigated in Appendix B.

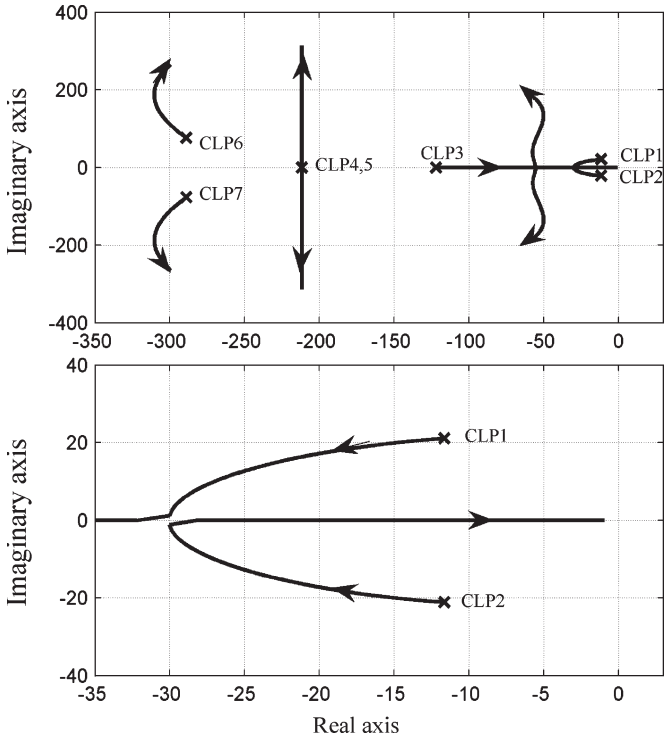

Fig. 3. Loci of closed-loop poles for simultaneous speed and stator-resistance estimation. $i_{sx} = 0$ A, $i_{sy} = +2$ A, and $\omega_e = 0.1 \rightarrow \pm 314$ elec. rad/s. Top subplot: complete Locus. Bottom subplot: zoom in at the origin.

B. Simultaneous Estimation of Motor-Speed and Rotor-Flux Magnitude: Scheme 2

This estimation scheme is most suitable for use at higher rotor speeds, where the effect of any stator-resistance mismatch is reduced. The adaptive error signals of the rotor-speed and the rotor-flux-magnitude estimation are defined by (6) as follows:

$$\varepsilon_\omega = -\frac{1}{a_2\hat{\psi}_r}\Delta i_{sy} \quad \varepsilon_\psi = -\frac{1}{a_2\omega_r^2}\Delta i_{sx}. \tag{16}$$

These adaptive error signals are fed to PI-type controllers to estimate ω_r, ψ_r, while the estimated value of a_1 is set equal to its nominal value. Thus

$$\hat{\omega}_r = G_{c\omega}\varepsilon_\omega \quad \hat{\psi}_r = G_{c\psi}\varepsilon_\psi \quad \hat{a}_1 = a_{1-n} \tag{17}$$

where $G_{c\psi} = k_{p\psi} + k_{i\psi}/s$. $k_{p\psi}$ and $k_{i\psi}$ are the PI controller gains.

1) Stability Analysis and Controller Design: By substituting from (6), about Δi_{sx} and Δi_{sy}, into (16), yields

$$\begin{bmatrix}\varepsilon_\omega \\ \varepsilon_\psi\end{bmatrix} = \begin{bmatrix}G_{\omega\omega} & G_{\omega\psi} \\ G_{\psi\omega} & G_{\psi\psi}\end{bmatrix}\begin{bmatrix}\Delta\omega_r \\ \Delta\psi_{rx}\end{bmatrix} + \begin{bmatrix}G_{\omega a1} \\ G_{\psi a1}\end{bmatrix}\Delta a_1 \tag{18}$$

where

$$G_{\psi\omega} = -\frac{a_1\hat{\psi}_r}{\omega_r sD} \quad G_{\psi\psi} = \frac{1}{D} \quad G_{\psi a1} = \frac{\hat{i}_{sx}(s+a_1) + \hat{i}_{sy}\omega_r}{a_2\omega_r^2 D}.$$

The rotor-speed and the rotor-flux-magnitude estimators, which are described by (16)–(18), are represented by a 2 × 2 MIMO closed-loop control system, as shown in Fig. 4. As in the previous sections, each estimator's PI controller is designed for independent use as a SISO closed-loop system. Subsequently, a stability investigation for simultaneous use is carried out.

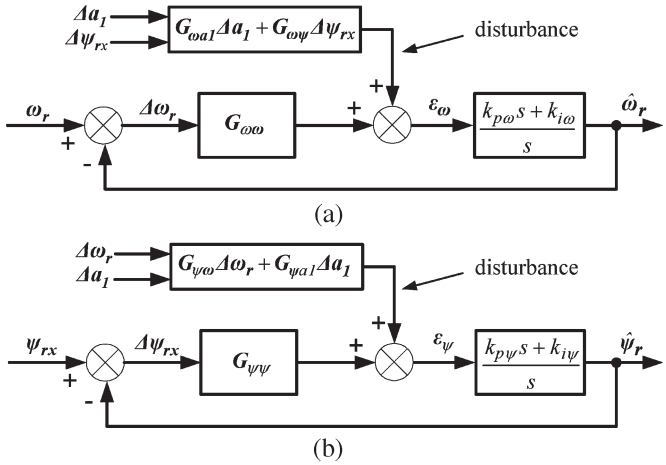

Fig. 4. Scheme-2 estimator block diagrams. (a) Rotor-speed estimator. (b) Rotor-flux estimator.

It should be noted from (16) that the speed estimator used in Scheme 2 is the same speed estimator used in Scheme 1. Therefore, the same PI controller gains will be used. Thus, the selected PI controller gains are the following: $k_{i\omega}/k_{p\omega} = a_1$ and $k_{p\omega} = 300$. Similarly, the rotor-flux-magnitude estimator transfer function $G_{\psi\psi}$ is equal to the stator-resistance estimator transfer function G_{a1a1}. Therefore, the same PI controller gains selected for the stator-resistance estimator are used here. Thus, the selected PI controller gains are the following: $k_{i\psi}/k_{p\psi} = 20$ and $k_{p\psi} = 5000$.

2) MIMO Stability Investigation: The stability of the two estimators when used simultaneously as a 2 × 2 MIMO system is investigated, using the PI controller gains selected in the previous section. From Fig. 4, the relationship between the system outputs $\hat{\omega}_r$ and $\hat{\psi}_r$ and the errors $\Delta\omega_r$ and $\Delta\psi_{rx}$, which represents the forward transfer function of the 2 × 2 MIMO system, is

$$\begin{bmatrix}\hat{\omega}_r \\ \hat{\psi}_r\end{bmatrix} = \begin{bmatrix}G_{c\omega} & 0 \\ 0 & G_{c\psi}\end{bmatrix} \times \left\{\begin{bmatrix}G_{\omega\omega} & G_{\omega\psi} \\ G_{\psi\omega} & G_{\psi\psi}\end{bmatrix}\begin{bmatrix}\Delta\omega_r \\ \Delta\psi_r\end{bmatrix} + \begin{bmatrix}G_{\omega a1} \\ G_{\psi a1}\end{bmatrix}\Delta a_1\right\}. \tag{19}$$

The effect of the error Δa_1 in (19) is assumed to be a bounded external disturbance, which is ignored for the stability study. The locations of the closed-loop poles of the 2 × 2 MIMO system are obtained by solving the characteristic equation

$$\left|\boldsymbol{I} + \begin{bmatrix}G_{c\omega} & 0 \\ 0 & G_{c\psi}\end{bmatrix}\begin{bmatrix}G_{\omega\omega} & G_{\omega\psi} \\ G_{\psi\omega} & G_{\psi\psi}\end{bmatrix}\right| = 0 \tag{20}$$

which is reduced to

$$1 + G_{c\omega}G_{\omega\omega} + G_{c\psi}G_{\psi\psi} + G_{c\omega}G_{c\psi}\lfloor G_{\omega\omega}G_{\psi\psi} - G_{\omega\psi}G_{\psi\omega}\rfloor = 0. \tag{21}$$

As in Section III-A4, the coefficients of the characteristic equation in (21) are found to be positive, then one of the Routh

stability conditions exists whatever the value of i_{sx}, since the polynomial coefficients of (21) are not functions of either i_{sx} or i_{sy}. In fact, if i_{sx} is set equal to zero in (14) and the same values of the PI controllers gains are used, the characteristic equations (21) and (14) are identical. Since the poles of (14) are stable, which are as shown in Fig. 3, the poles of (21) are also stable. In conclusion, the two estimators of Scheme 2, when acting together, show stable operation at any operating point, independent of the values of i_{sx} and i_{sy}. The convergence of the Scheme-2 estimators is investigated in Appendix B.

IV. Experimental Results

The algorithm of the sensorless IRFOC PMSM drive incorporating the designed rotor-speed, stator-resistance, and rotor-flux-magnitude MRAS estimators has been implemented on a TMS320C31 DSP platform. The pulsewidth-modulation (PWM) switching and the current sampling are synchronized to a common interval of 100 μs, so there is no need for filtering of the current signals. The stator voltage is reconstructed by using the PWM pulses and the measured dc link voltage. In addition, an algorithm is implemented to compensate the effect of the inverter nonlinearities, i.e., the dead time and the device voltage drops [19]. The discussion of the algorithm is beyond the scope of this paper. An incremental position encoder of 4096 lines is used to measure the rotor position. The measured rotor position is used for comparison purpose only. The (adjustable) model of the PMSM implemented inside the control algorithm should strictly include the effects of harmonics in the spatial distribution of the magnet flux and of the air-gap reluctance variations due to the stator slots. These effects are sources of current harmonics and torque pulsations. However, the PMSM used for the experimental investigation had a sinusoidally distributed magnet flux and skewed stator slots, so the flux harmonics and air-gap reluctance variations are negligible, and thus, the ideal machine model can be used. The stator current, rotor speed, rotor position, stator resistance, and rotor flux are estimated using (5), (8), and (17), respectively. Extensive experimental work has been carried out to investigate the performance and the stability of the developed PMSM drive at low-speed operation, using Scheme 1 in comparison with Scheme 2. The parameters of the PMSM used for the experimental work are given in Appendix A.

An initial set of tests were carried out with the drive being used to lift and lower a constant mass (crane-type load). During the lifting phase, the PMSM operates in motoring mode, while it operates in generating mode during lowering. The drive lifts a mass of 15 kg at the low speed of 2 rad/s. The reference value of i_{sx} is set equal to zero.

For the results shown in Fig. 5, the estimators of Scheme 1 were activated with the estimated rotor-flux-magnitude set constant at 0.24 W. At $t = 0$ s, the speed is reversed to -2 rad/s to lower down the load. The average value of the rotor-position error converges to zero, as shown in Fig. 5(c). Despite the high system noise-to-signal ratio during such low-speed operation, the results show stable operation in motoring and generating modes. With an improved inverter-nonlinearity-compensation algorithm, smoother and smaller ripple signals could be obtained at low speeds. The torque current component i_{sy} is shown in Fig. 5(f). During the lifting period, i_{sy} was greater than 3 A, which corresponds to 90% of the rated torque of the motor. In the lowering period, i_{sy} is less than 3 A because of the crane-pulley friction-torque component being reversed. The estimated stator resistance is shown in Fig. 5(d). Its value is almost unchanged by the speed reversal, since its sensitivity to machine parameter mismatch is small at low speeds [see (B.3)].

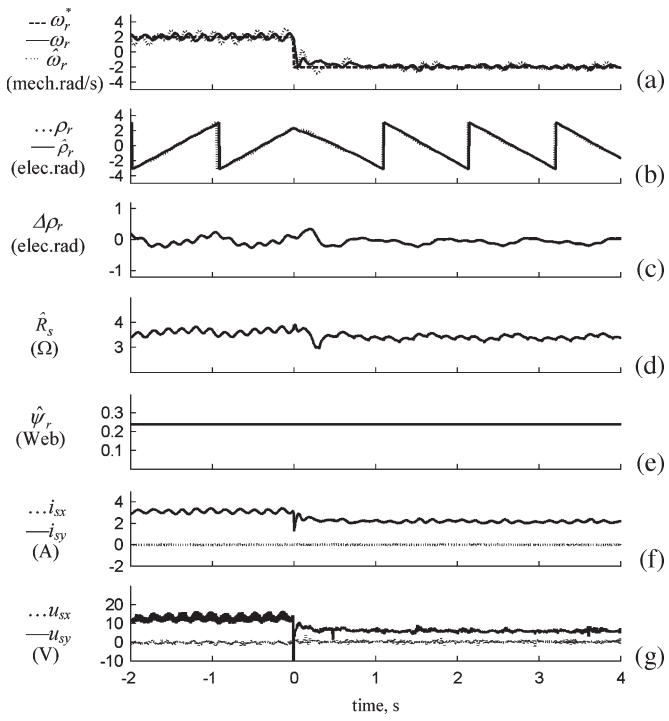

Fig. 5. Experimental results, Scheme 1, crane load. Operation at low speeds with nominal value of rotor flux.

When the same test was carried out but with the Scheme 2 estimators activated, with the estimated stator-resistance value set constant and equal to its nominal value, the results obtained are shown in Fig. 6. The results show stable operation in motoring and generating modes. It is also noted that the average value of the rotor-position error converges to zero, as shown in Fig. 7(c). Thus, Schemes 1 and 2 exhibit satisfactory responses in this initial experiment.

The effect of errors in the quantity that is not being estimated was investigated by the next pair of experiments. First, Scheme 1 was applied with the same test conditions used to obtain the results in Fig. 5 but with a detuned rotor flux magnitude (set to 170% of its rated value). The results in Fig. 7 show stable operation of the sensorless Scheme 1, even with such a large rotor-flux mismatch. Note, however, that the estimated stator-resistance value is increased after the speed reversal because of the rotor-flux mismatch. A similar test was carried out using Scheme 2. The experimental conditions were the same, as though used when obtaining the results in Fig. 6, except that the stator resistance was detuned by setting it to 95% of the correct value. The results in Fig. 8 show unstable behavior during transient period after the speed-reversal moment at $t = 0$ s. At the low rotor speed, the sensorless Scheme 2 shows great sensitivity to even a small stator-resistance mismatch of 5%.

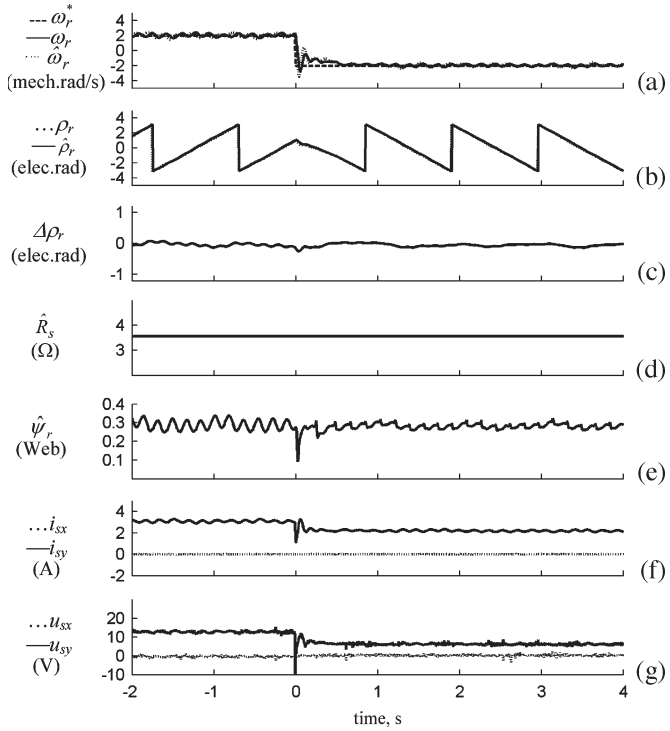

Fig. 6. Experimental results, Scheme 2, crane load. Operation at low speed with nominal value of stator resistance.

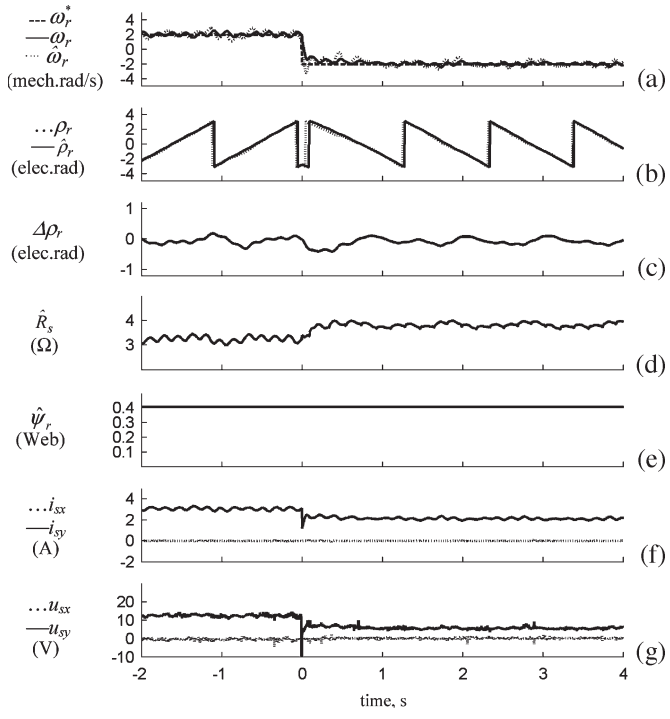

Fig. 7. Experimental results, Scheme 1, crane load. Low-speed operation with rotor flux at 170% of nominal value.

Another common test for sensorless drives is to investigate the convergence of the estimated rotor position to the true value during the start up of the drive. In this test, the PMSM motor was coupled to a dc generator, which acted as a load. The dc-generator terminals were connected to a resistor, causing the load torque at the motor shaft to be proportional to rotor speed.

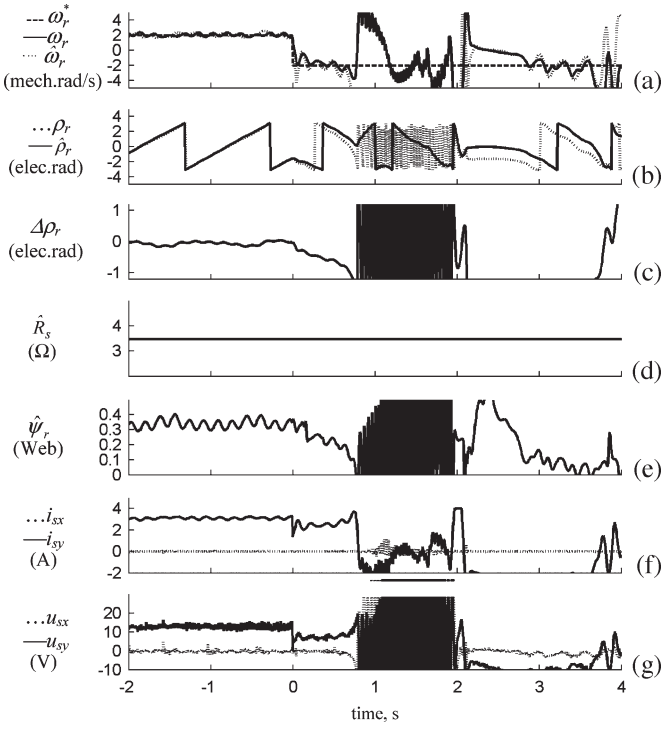

Fig. 8. Experimental results, Scheme 2, crane load. Low-speed operation with stator resistance set at 95% of nominal value.

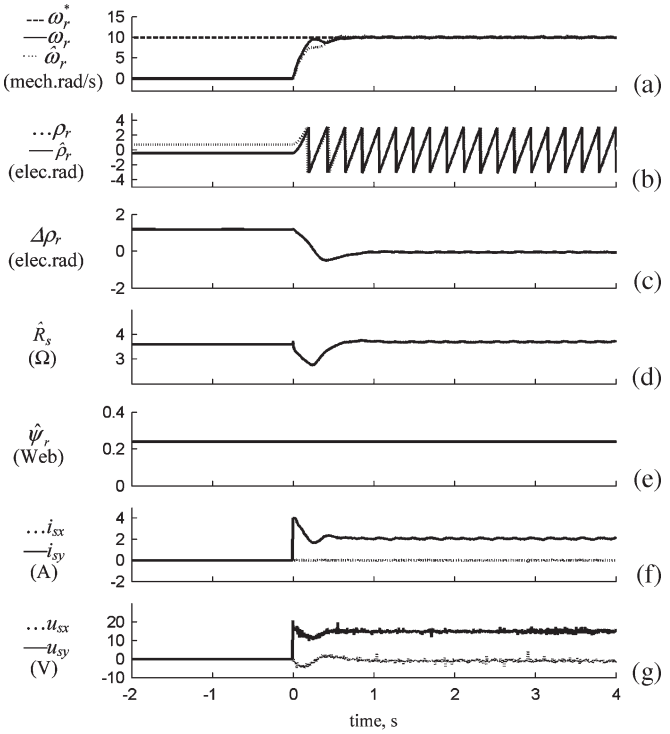

Fig. 9. Experimental results, Scheme 1 with speed-dependent load. Effect of initial position error using nominal value of rotor flux.

First, Scheme 1 was investigated. The rotor flux magnitude was set equal to its rated value. The reference speed was set to 10 rad/s. The initial rotor-position error was set to $+1.2$ elec. rad. The drive and the estimators were started at $t = 0$ s. The results obtained are shown in Fig. 9, which demonstrates that the

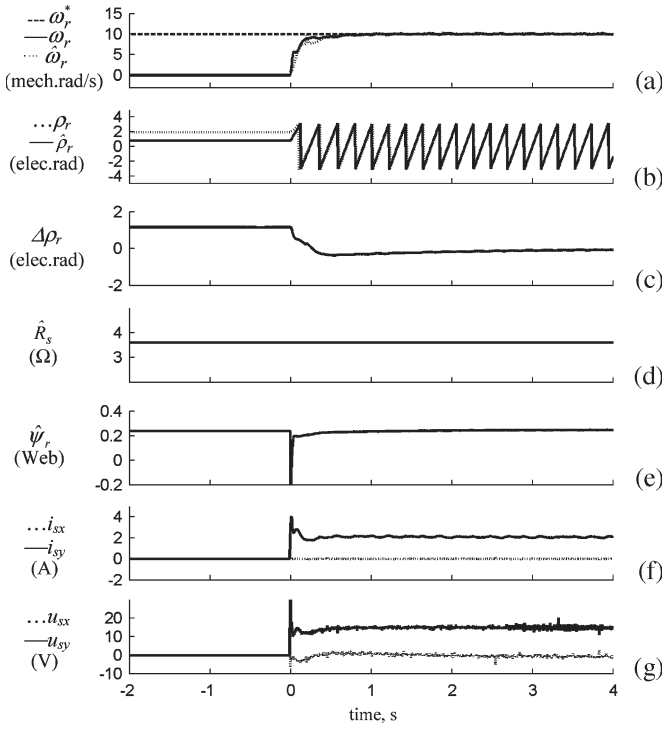

Fig. 10. Experimental results, Scheme 2 with speed-dependent load. Effect of initial position error using nominal value of stator resistance.

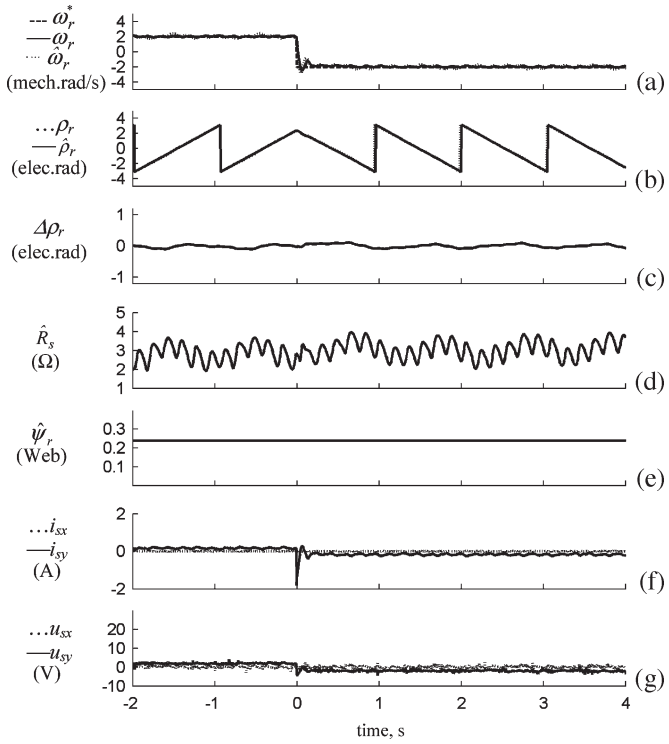

Fig. 11. Experimental results, Scheme 1 at low speed and light load.

rotor position converges quickly to its correct value. It can be seen from the results that, at higher speed operation, the noise-to-signal ratio is less. The same experimental conditions were used for Scheme 2 but with the stator resistance set to its rated value. The results obtained are shown in Fig. 10, where it can be seen that the rotor-position error reduces to zero within 0.5 s.

Finally, the two schemes were investigated for no-load operation. In this test, the shaft of the PMSM was completely decoupled from the shaft of the dc generator and left to run free of load. A speed-reversal test from 2 to -2 rad/s was carried out for Scheme 1 with the rotor flux magnitude set to its rated value. The results obtained (Fig. 11) show stable operation. The average value of the rotor-position error tended to zero. Although, i_{sy} was very small [Fig. 11(f)], stable stator-resistance estimation was still possible [Fig. 11(d)]. The relatively high ripple content of the stator-resistance estimate is due to the high noise-to-signal ratio of the reconstructed stator voltage. When the same test was carried out for Scheme 2, with the stator resistance at its rated value, the results obtained were as shown in Fig. 12. Again the results are stable, but the cyclic variation of the position error [Fig. 12(c)] is larger than that occurring in the Scheme 1 results [Fig. 11(c)], because Scheme 2 is less suitable for such low-speed operation.

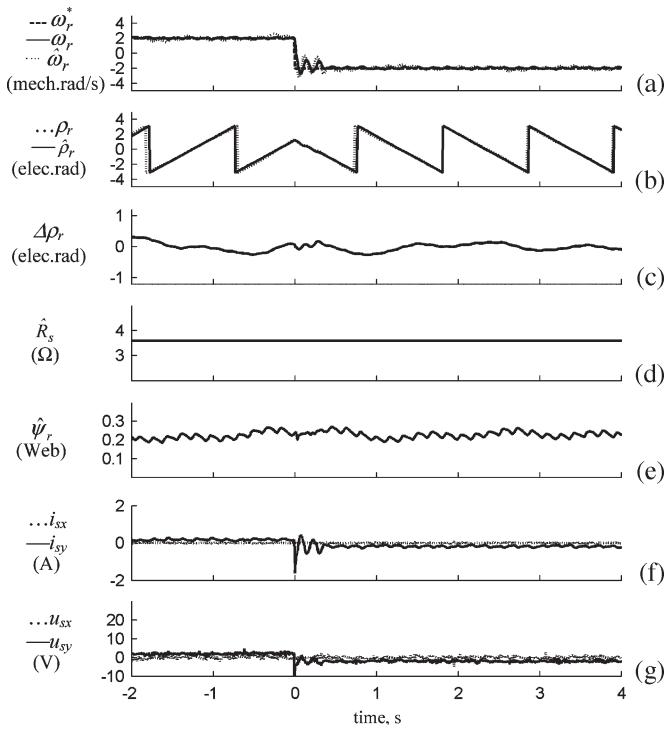

Fig. 12. Experimental results, Scheme 2 at low speed and light load.

V. Conclusion

The proposed sensorless IRFOC PMSM drive provides a rotor-position estimate, which is immune to system noise, and an accurate speed estimate, which is insensitive to machine-parameter mismatch. The rotor speed, the rotor flux magnitude, and the stator resistance have been regarded as slowly varying parameters, which have been adaptively estimated using three MRAS estimators. It has been demonstrated that simultaneous estimation of the stator resistance and the rotor flux magnitude is not possible in sensorless PMSM drives. Two sensorless schemes, Schemes 1 and 2, have been proposed. In Scheme 1, the rotor speed and the stator resistance are estimated, while in

Scheme 2, the rotor speed and the rotor flux magnitude are the estimated quantities. It has been demonstrated by theoretical and experimental investigations that Scheme 1 is more suitable for low-speed operation than Scheme 2, since Scheme 2 is very sensitive to stator-resistance mismatch at low-speed operation. Stability analysis and design based on the linear-control theory have been performed for the proposed MRAS estimators on an independent and simultaneous use basis. The convergence of the estimated quantities to their true values is also guaranteed on the condition that the other machine parameters are accurately known. The convergence of the estimated rotor position to its true value is always possible if i_{sx} is equal to zero, whatever the value of the machine-parameter mismatch. Experimental investigations of the drive demonstrate that accurate and stable position/speed estimation is possible in the various operating modes, provided that an appropriate estimation scheme is chosen.

APPENDIX A
PMSM PARAMETERS

Connection type	Y;
rated voltage	380 V;
rated current	3.54 A;
number of phases	3;
number of poles	6;
frequency	50 Hz;
rated speed	3000 r/min;
L_s	0.017 H;
R_s	3.6 Ω;
ψ_{r-n}	0.24 W;
maximum torque ($T_{e-\max}$)	5 N·m;
rated torque (T_{e-n})	3.7 N·m.

APPENDIX B
PROOF OF CONVERGENCE

Scheme 1

The stable operation of the two estimators of Scheme 1 when used independently is guaranteed, as demonstrated in Section III-A4. However, it is crucial for high-performance/efficient operation of sensorless PMSM drive that the steady-state errors of the estimated quantities converge to zero. At steady state, the adaptive error signals ε_ω and ε_{a1} are equal to zero since they are fed to PI controllers. In addition, the estimated speed is exactly equal to the actual speed; thus, the speed error is zero, as has been explained in Section III-A2. Then, at steady state: $\varepsilon_\omega = 0$; $\varepsilon_{a1} = 0$; and $\Delta\omega_r = 0$; also, $\hat{\omega}_r = \omega_e = \omega_r$, $\hat{i}_{sx} = i_{sx}$, and $\hat{i}_{sy} = i_{sy}$. Furthermore, practically the set value of the estimated flux magnitude $\hat{\psi}_r$ is not exactly equal to the actual value of the magnet flux ψ_r. The difference between the square of the actual magnet flux ψ_r^2 and the square of the estimated magnitude $\hat{\psi}_r^2$ is assumed equal to δ, i.e., $\psi_r^2 - \hat{\psi}_r^2 = \delta$, and from which the following is obtained:

$$2\hat{\psi}_r \Delta\psi_{rx} + \left(\Delta\psi_{rx}^2 + \Delta\psi_{ry}^2\right) = \delta. \tag{B.1}$$

In addition, by substituting (4b) into (7) and by substituting the operator $s = 0$, yields

$$\varepsilon_\omega = (a_1 i_{sy} - \omega_r i_{sx})\Delta a_1 + a_1 a_2 \omega_r \Delta\psi_{rx} + a_2 \omega_r^2 \Delta\psi_{ry} = 0 \tag{B.2a}$$

$$\varepsilon_{a1} = i_s^2 \omega_r \Delta a_1 + a_2 \omega_r (\omega_r i_{sy} - a_1 i_{sx})\Delta\psi_{rx} - a_2 \omega_r (\omega_r i_{sx} + a_1 i_{sy})\Delta\psi_{ry} = 0. \tag{B.2b}$$

From (B.1) and (B.2), the errors $\Delta\psi_{rx}$, $\Delta\psi_{ry}$, and Δa_1, as functions of δ, are

$$\Delta\psi_{rx} = \frac{i_{sy}^2 \hat{\psi}_r}{\left(i_{sx}^2 + i_{sy}^2\right)} \left(-1 \pm \sqrt{\frac{\hat{\psi}_r^2 i_{sy}^2 + \left(i_{sx}^2 + i_{sy}^2\right)\delta}{\hat{\psi}_r^2 i_{sy}^2}} \right) \tag{B.3a}$$

$$\Delta\psi_{ry} = -\frac{i_{sx}}{i_{sy}} \Delta\psi_{rx} \tag{B.3b}$$

$$\Delta a_1 = -\frac{a_2 \omega_r}{i_{sy}} \Delta\psi_{rx} = -\frac{a_2 \omega_r i_{sy} \hat{\psi}_r}{\left(i_{sx}^2 + i_{sy}^2\right)} \left(-1 \pm \sqrt{\frac{\hat{\psi}_r^2 i_{sy}^2 + \left(i_{sx}^2 + i_{sy}^2\right)\delta}{\hat{\psi}_r^2 i_{sy}^2}} \right) \tag{B.3c}$$

$$\Delta\rho_r = \sin^{-1}\left(\frac{\Delta\psi_{ry}}{\psi_r}\right). \tag{B.3d}$$

It should be noted from (B.3b) that, if i_{sx} is equal to zero, $\Delta\psi_{r\psi}$ is also zero whatever the value of δ. In addition, from (B.3d), the error in the estimated rotor position $\Delta\rho_r$ is either zero or $\pm\pi$ rad. However, if the estimators are activated when the initial position uncertainty is less than $\pm\pi/2$ rad, $\Delta\rho_r$ usually converges to zero. Then, if i_{sx} is zero, the steady-state errors are

$$\Delta\psi_{rx} = \gamma,\ \Delta\psi_{ry} = 0,\ \Delta R_s = -\frac{\omega_r}{i_{sy}}\gamma, \text{ and } \Delta\rho_r = 0 \tag{B.4}$$

where $\gamma = (\psi_r - \hat{\psi}_r)$.

It should be noted from (B.4) that $\Delta\rho_r$ is zero despite the value of the rotor-flux-magnitude mismatch γ. However, the error in the estimated stator resistance is proportional to γ, ω_r, and the inverse of i_{sy}. Practically, the change in γ during operation is small, and thus, its effect on the estimation accuracy is small. If γ is equal to zero, i.e., $\hat{\psi}_r$ is set exactly equal to the true value, the estimated stator resistance converges to its true value. In addition, theoretically, at no-load, when $i_{sy} \to 0$ A and $i_{sx} = 0$ A, the error in the estimated stator resistance tends to infinity. But, practically, i_{sy} exists even when the PMSM operates at no-load. In general, the reference value of i_{sx} is set equal to zero in order to obtain accurate rotor-position estimate even when γ exists.

Scheme 2

The convergence of the rotor-flux vector to its true value and the influence of the stator-resistance mismatch Δa_1 on the estimate of the rotor flux magnitude and position must be investigated. At steady state, the adaptive error signals ε_ω and ε_ψ and the speed error $\Delta\omega_r$ are equal to zero. Then, by substituting (4b) into (16) and setting the operator $s = 0$

$$\varepsilon_\omega = (a_1 i_{sy} - \omega_r i_{sx})\Delta a_1 + a_1 a_2 \omega_r \Delta\psi_{rx} + a_2 \omega_r^2 \Delta\psi_{ry} = 0 \tag{B.5a}$$

$$\varepsilon_\psi = (-a_1 i_{sx} - \omega_r i_{sy})\Delta a_1 - a_2 \omega_r^2 \Delta\psi_{rx} + a_1 a_2 \omega_r \Delta\psi_{ry} = 0. \tag{B.5b}$$

By solving (B.5), the rotor-flux-vector error components as functions of Δa_1 are

$$\Delta\psi_{ry} = (i_{sx}/a_2\omega_r)\Delta a_1 \tag{B.6a}$$

$$\Delta\psi_{rx} = -(i_{sy}/a_2\omega_r)\Delta a_1. \tag{B.6b}$$

It should be noted from (B.6a) that, if i_{sx} is zero, $\Delta\psi_{r\psi} \to 0$, and, thus,

$$\Delta\rho_r = 0 \quad \psi_{ry} = 0,$$

$$\psi_{rx} = \psi_r \; \Delta\psi_{rx} = (\psi_r - \hat{\psi}_r) = -\frac{i_{sy}}{\omega_r}\Delta R_s. \tag{B.7}$$

From (B.7), the rotor-position error is zero despite the stator-resistance mismatch: The existence of Δa_1 influences only the error in the estimate of the rotor flux magnitude $\Delta\psi_{rx}$. The error $\Delta\psi_{rx}$ increases as the speed decreases down to zero. However, the influence of Δa_1 is small at high speeds. Even if i_{sx} is nonzero, the influence of Δa_1 on the rotor-position and rotor-flux-magnitude estimate tends to zero as ω_r tends to infinity, so Scheme 2 is more suitable for high-speed operation.

REFERENCES

[1] J. Kim and S. Sul, "New approach for high performance PMSM drives without rotational position sensors," *IEEE Trans. Power Electron.*, vol. 12, no. 5, pp. 904–911, Sep. 1997.

[2] N. Matsui and M. Shigyo, "Brushless dc motor control without position and speed sensors," *IEEE Trans. Ind. Appl.*, vol. 28, no. 1, pp. 120–127, Jan./Feb. 1992.

[3] N. Matsui, "Sensorless PM brushless dc motor drives," *IEEE Trans. Ind. Electron.*, vol. 43, no. 2, pp. 300–308, Apr. 1996.

[4] N. Ertugrul and P. Acarnley, "A new algorithm for sensorless operation of permanent magnet motors," *IEEE Trans. Ind. Appl.*, vol. 30, no. 1, pp. 126–133, Jan./Feb. 1994.

[5] J. Solsona, M. I. Valla, and C. Muravchik, "A nonlinear reduced order observer for permanent magnet synchronous motors," *IEEE Trans. Ind. Electron.*, vol. 43, no. 4, pp. 492–497, Aug. 1996.

[6] J. Solsona and M. I. Valla, "Disturbance and nonlinear luenberger observers for estimating mechanical variables in permanent magnet synchronous motors under mechanical parameters uncertainties," *IEEE Trans. Ind. Electron.*, vol. 50, no. 4, pp. 717–725, Aug. 2003.

[7] M. Tomita, T. Senjyu, S. Doki, and S. Okuma, "New sensorless control for brushless DC motors using disturbance observers and adaptive velocity estimators," *IEEE Trans. Ind. Electron.*, vol. 45, no. 2, pp. 274–282, Apr. 1998.

[8] Z. Chen, M. Tomita, S. Doki, and S. Okuma, "An extended electromotive force model for sensorless control of interior permanent-magnet synchronous motors," *IEEE Trans. Ind. Electron.*, vol. 50, no. 2, pp. 288–295, Apr. 2003.

[9] S. Ichikawa, Z. Chen, M. Tomita, S. Doki, and S. Okuma, "Sensorless controls of salient-pole permanent magnet synchronous motors using extended electromotive force models," *Electr. Eng. Jpn.*, vol. 146, no. 3, pp. 55–64, 2004.

[10] Z. Chen, M. Tomita, S. Doki, and S. Okuma, "New adaptive sliding observers for position and velocity-sensorless controls of brushless DC motors," *IEEE Trans. Ind. Electron.*, vol. 47, no. 3, pp. 582–591, Jun. 2000.

[11] S. Shinnaka, "New sensorless vector control using minimum-order flux state observer in a stationary reference frame for permanent-magnet synchronous motors," *IEEE Trans. Ind. Electron.*, vol. 53, no. 2, pp. 388–398, Apr. 2006.

[12] L. A. Jones and J. H. Lang, "A state observer for the permanent-magnet synchronous motor," *IEEE Trans. Ind. Electron.*, vol. 36, no. 3, pp. 374–382, Aug. 1989.

[13] J. Solsona, M. I. Valla, and C. Muravchik, "Nonlinear control of a permanent magnet synchronous motor with disturbance torque estimation," *IEEE Trans. Energy Convers.*, vol. 15, no. 2, pp. 163–168, Jun. 2000.

[14] R. B. Sepe and J. H. Lang, "Real-time observer-based (adaptive) control of a permanent-magnet synchronous motor without mechanical sensors," *IEEE Trans. Ind. Appl.*, vol. 28, no. 6, pp. 1345–1352, Nov. 1992.

[15] T. S. Low, T. H. Lee, and K. T. Chang, "A nonlinear speed observer for permanent-magnet synchronous motors," *IEEE Trans. Ind. Electron.*, vol. 40, no. 3, pp. 307–316, Jun. 1993.

[16] S. Bolognani, R. Oboe, and M. Zigliotto, "Sensorless full-digital PMSM drive with EKF estimation of speed and rotor position," *IEEE Trans. Ind. Electron.*, vol. 46, no. 1, pp. 184–191, Feb. 1999.

[17] M. Boussak, "Implementation and experimental investigation of sensorless speed control with initial rotor position estimation for interior permanent magnet synchronous motor drive," *IEEE Trans. Power Electron.*, vol. 6, no. 6, pp. 1413–1422, Nov. 2005.

[18] C. Schauder, "Adaptive speed identification for vector control of induction motors without rotational transducers," *IEEE Trans. Ind. Appl.*, vol. 28, no. 5, pp. 1054–1061, Sep./Oct. 1992.

[19] J. W. Choi and S. K. Sul, "Inverter output voltage synthesis using novel dead time compensation," *IEEE Trans. Power Electron.*, vol. 11, no. 2, pp. 221–227, Mar. 1996.

Mohamed Rashed received the B.Sc. and M.Sc. degrees in electrical engineering from Mansoura University, Mansoura, Egypt, in 1987 and 1993, respectively, and the Ph.D. degree in electrical engineering from University of Aberdeen, Aberdeen, U.K., in 2002.

He was a Postdoctoral Fellow with the Department of Engineering, University of Aberdeen, between 2002 and 2005. He is currently a Lecturer in the Electrical Engineering Department, Mansoura University. His fields of interest are in the control of electrical drives and power electronics of grid-connected renewable-energy sources, including the development of artificial-intelligence-based, self-tuning, sliding-mode, adaptive-inverse, and sensorless-control algorithms for power electronics and electrical drive systems.

Peter F. A. MacConnell received the M.Eng. degree from the University of Strathclyde, Glasgow, U.K., in 1988, and the Ph.D. degree from the University of Exeter, Exeter, U.K., in 1995.

He was with the Department of Engineering, University of Aberdeen, Aberdeen, U.K., in 1996, where he is currently a member of the Dynamics and Control Research Group. His principal research interest is the application of artificial intelligence to oil- and gas-industry control problems. A complementary interest to that is his research on the control and condition monitoring of electric machines with particular interest in sensorless control. In addition, as part of a U.K.-wide network, he is investigating the use of artificial intelligence for pattern recognition of biological and clinical data.

A. Fraser Stronach received the B.Sc.(Eng.) degree in mechanical engineering and the Ph.D. degree in power systems from the University of Aberdeen, Aberdeen, U.K., in 1988 and 1995, respectively.

He was previously a Senior Lecturer in engineering in the Department of Engineering, University of Aberdeen. He is currently a self-employed, trading under the name Genbase Information Systems, Aberdeen. His research interests included development of artificial-intelligence-based methods for control of electromechanical drives and for the monitoring of electromechanical systems, application of artificial-intelligence-based methods for monitoring and control for oil-industry-related processes, and development of offshore and shipborne electrical power system simulation software. His teaching interests spanned control systems, electromechanical systems, engineering mathematics, digital systems, and computing.

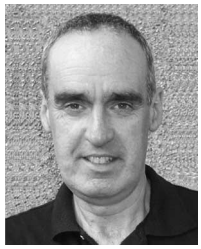

Paul Acarnley received the B.Sc. and Ph.D. degrees in electrical engineering from Leeds University, Leeds, U.K., in 1974 and 1977, respectively, and the M.A. degree from Cambridge University, Cambridge, U.K., in 1978.

After seven years in the Department of Engineering, Cambridge University, he was with the Power Electronics, Drives, and Machines Group, University of Newcastle upon Tyne, Newcastle upon Tyne, U.K., in 1986. In 2003, he founded the Research Engineering Education Services, Stonehaven, U.K. He is currently a Research Professor in the School of Engineering, Robert Gordon University, Aberdeen, U.K., and at the University of Aberdeen, Aberdeen, and an Emeritus Professor at the University of Newcastle upon Tyne. He is the author of *Stepping Motors: A Guide to Theory and Practice* (Institution of Electrical Engineers, 1982; 4th ed., 2002). His principal research interest is in the control of electric drives, including work on state and parameter estimation applied to torque, current, temperature, speed and position estimation in motors, and temperature estimation in power electronic devices. In addition, he has made contributions in the areas of stepping motors, permanent-magnet generators, flywheel energy storage, and brushless dc drives.

Dr. Acarnley is a Fellow of the Institution of Electrical Engineers, U.K.